ELSEVIER

Journal of Wind Engineering
and Industrial Aerodynamics 62 (1996) 57–79

JOURNAL OF
wind engineering
AND
industrial
aerodynamics

Numerical and experimental study of the flow over a two-dimensional car model

W. Angelis, D. Drikakis*,[1], F. Durst*, W. Khier

Institute of Fluid Mechanics, University of Erlangen-Nuremberg, Cauerstr. 4, D-91058 Erlangen, Germany

Received 23 June 1995; revised 25 April 1996; accepted 9 September 1996

Abstract

A numerical and experimental study of the flow over a two-dimensional car model in proximity to the ground is presented. Velocity measurements around the car have been obtained in a wind tunnel using laser-Doppler-anemometry. Pressure measurements on the upper and lower car surfaces have also been performed. The experimental measurements are compared with numerical predictions. The numerical method is based on a pressure correction algorithm of the SIMPLE-type. A multigrid technique, based on the full approximation storage (FAS) scheme is employed to accelerate the numerical convergence, while as a turbulence model the standard k–ε model with wall functions is used. Comparisons between numerical and experimental results for the u and v velocity profiles, as well as, for the pressure distribution over the car surface are presented.

1. Introduction

Study of the flow over car geometries can be performed by experiments in wind tunnels, as well as by numerical simulation. Wind tunnels have been extensively used for years in automobile aerodynamics in order to improve modern vehicle design [1,2]. In the past, experiments mainly involved the measurement of the aerodynamic coefficients and flow visualization over vehicles. Bearman [3] performed wind-tunnel experiments to measure the wakes of model vehicles. Rauser et al. [4] performed wind-tunnel tests using 1/5-scale basic vehicle structures. They investigated the effects of underbody design on vehicle aerodynamics and found solutions for application to series production. Their experiments showed that it is possible to further improve the aerodynamics of production-type bodies by adding an efficient underbody panelling.

* Corresponding authors.
[1] Present address: UMIST, Department of Mechanical Engineering, PO Box 88, Manchester M60, UK.

PII S0167-6105(96)00053-0

Such configurations were already employed for racing cars, but not to vehicles for everyday use. Ahmed [5,6] performed a series of wind-tunnel experiments in order to examine the wake structure of a realistic automobile model. He studied the time-averaged wake structure on the basis of flow visualization and wake surveys behind smooth quarter scale models. Ahmed et al. [7] also performed experiments with a bluff-body, "basic-ground", vehicle. They presented pressure measurements, wake surveys and force measurements for different angles of base-slant. They showed that almost 85% of body drag is pressure drag and most of this drag is generated at the rear end. They also showed that wake flow exhibits a triple-deck system of horseshoe vortices, where the strength and existence of these depend upon the base-slant angle. Although various experimental studies have been carried out in the field of car aerodynamics there is still lack of experimental measurements using advanced instrumentation techniques such as laser-Doppler-anemometry [8].

During the recent past, significant progress in the field of computational fluid dynamics (CFD) has also been made, and CFD is gradually becoming established as an efficient tool in vehicle design. The majority of numerical investigations in the field of car aerodynamics have been concerned with grid generation problems around complex three-dimensional geometries, as well as, with the prediction of the aerodynamic coefficients. Takagi [9] presented a review of the applications of computers to automobile aerodynamics, including external flow over car geometries, flow in passenger compartments and flow in engine cylinders. Reviews of CFD methods used in automobile aerodynamics have also been published by Kobayashi et al. [10] and Rieger et al. [11]. The research efforts of several other authors in this field can be found in the references of the above review papers. Shaw [12] compared different commercial CFD packages and concluded that although the aerodynamic forces were not well predicted, the quantitative flow structure was realistic. Han [13] performed computations over a three-dimensional bluff-body in proximity to the ground. Due to the lack of detailed velocity measurements over this body, he compared qualitatively the formation of the vortices in the wake and the drag coefficient for different slant angles. He reported that the overall validity of the computations was dependent on the turbulence model and the accuracy of the discretisation scheme. His computations revealed that the standard k–ε model with wall functions consistently underpredicted the base pressure.

Some of the problems related to CFD in the automobile industry are grid generation, turbulence modelling, accuracy of the numerical scheme (see Ref. [10]), computer requirements and, finally, experimental data for the validation of CFD codes over such geometries.

The objective of the present work is to undertake a complimentary experimental and numerical investigation of the flow over a two-dimensional car model. Pressure measurements have been obtained on the upper and lower car surfaces while measurements of the u and v velocity components have been performed using the LDA technique [8]. Experimental velocity profiles are presented at different positions around the car geometry. Numerical simulation has also been performed using an incompressible Navier–Stokes code which is based on a pressure correction algorithm of the SIMPLE-type.

In Sections 2 and 3, respectively, the experimental facility and numerical method are described. Numerical and experimental results are presented in Section 4. Finally, in Section 5 the conclusions from the present work are summarised.

2. Description of experiments

2.1. Wind tunnel

The experiments were performed in a wind tunnel, which is 3/4 open at the sides and the top (Figs. 1 and 2). The highest air-speed the wind tunnel can reach is 55 m/s,

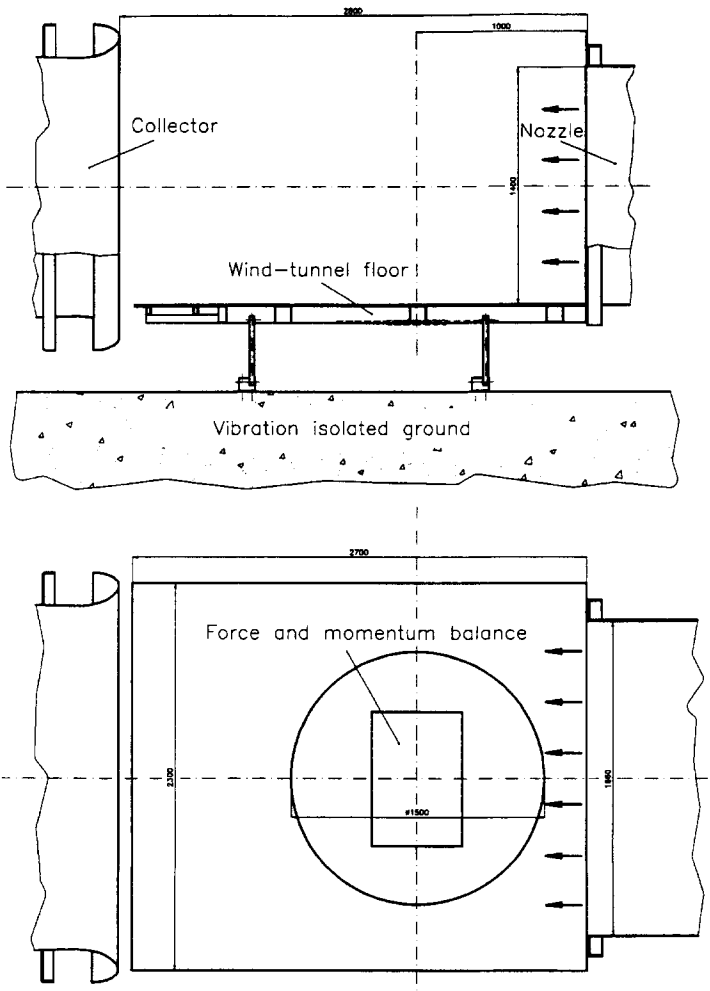

Fig. 1. Side and plan views of the wind tunnel.

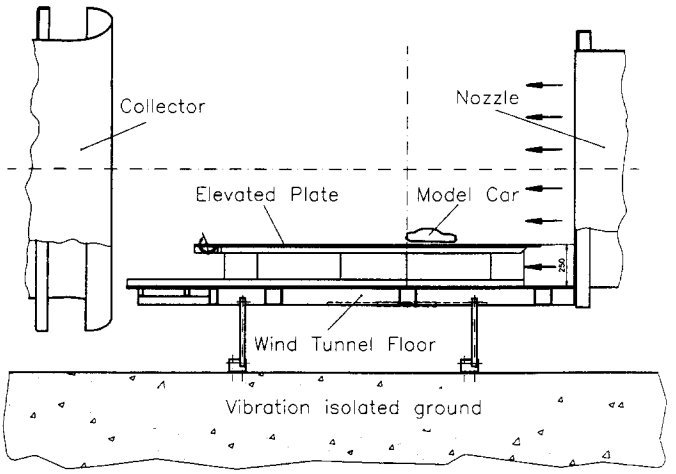

Fig. 2. Side view of the wind tunnel with the car model and the flat plate as ground.

Table 1
Specification of the LDA system

Focal length	400 mm
Control volume (CV) diameter	75 μm
Control volume length	1.6 mm
Laser light power in the CV	400 mm
Used light wave lengths	514 nm, 488 nm

and the turbulence level is less than 0.3%. The length, height and span of the test section are 2.8, 1.4 and 1.8 m, respectively. For positioning the probes in the wind tunnel, and for turning the wind tunnel ground-table, a seven-axis traversing system is used. The inaccuracies of the linear and the angular traversing (i.e. the ground table) are less than 0.05 mm and 0.2°, respectively. The data acquisition and processing is done by a PC. For LDA measurements the commercial BURSTWARE software by Dantec is used. For hot-wire measurements, a software package was developed [14].

2.2. *Velocity measurements*

For simultaneous measurement of the two velocity components around the car model an LDA system was used. The specification of this system is shown in Table 1. In order to keep the measuring time as short as possible, the air flow in the test section was seeded by fluid particles of DEHS with diameter between 1 and 2 μm. Hot-wire measurements (X-wire and boundary layer probes) were also used for determining the inflow quantities. These probes were supplied by hot-wire-bridges (DANTEC 55M), which were run in the constant-temperature mode. The frequency

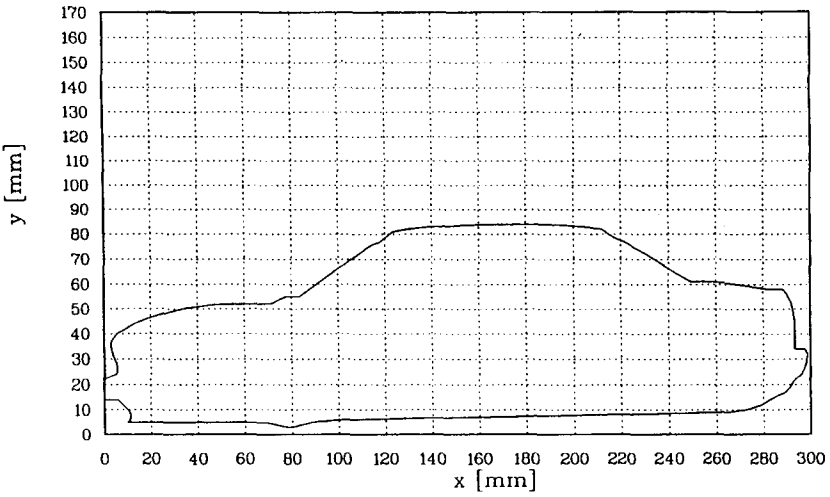

Fig. 3. Car model geometry.

response of the whole system was up to 40 kHz. In the case of mean velocity masurements the output signal of the hot-wire bridge was directly acquired by a 16-bit A/D-converter-card. For measuring the turbulence quantities, a backup-amplifier with a low-pass-filter (10 kHz) was switched between the hot-wire bridge and A/D-converter-card. The task of this backup amplifier was to remove the DC-part of the hot-wire signal and to amplify the remaining AC-part by a constant factor of 50.

2.3. *Pressure measurements*

For measuring the pressure on the surface of the car, 36 pressure holes were drilled in the model. Tubes of brass with 2 mm outer and 0.8 mm inner diameter were fixed in these holes and very carefully made flush with the model surface. The surface pressure was transferred to the measuring unit by flexible tubes on the inner side of the car model. A pressure measuring unit (SETRA Type 239) with a maximum differential pressure of 127 mm water, an accuracy of 0.14% FS and an output voltage of 0 to 5 V DC, was used.

The reference pressure was the static pressure of the free stream in the wind tunnel. For measuring the static pressure along the flat plate, a Prandtl tube was fixed to the wind tunnel traversing unit and positioned in the spanwise middle plane of the wind tunnel, 5 cm above the plate.

2.4. *Description of the model and boundary conditions*

A two-dimensional car model was constructed (Fig. 3). The x and y coordinates of the geometry are given in Table 2. The present geometry has a cross-sectional shape of a typical passenger car. The dimensions are 295 mm in the streamwise direction,

Table 2
Coordinates of the car model

x (mm)	y (mm)	x (mm)	y (mm)	x (mm)	y (mm)
0.	14.00288	292.2945	48.64162	109.9315	73.45375
5.52226	13.63439	290.8818	53.55491	107.363	71.3656
8.47603	11.30057	288.827	57.11705	104.7945	69.64595
8.47603	11.30057	285.7448	57.36271	99.5291	66.08381
10.91609	8.22977	282.6626	57.23988	94.39212	62.76734
10.91609	6.26445	279.452	57.73121	87.5856	58.22254
9.8887	4.66763	275.9845	58.22254	82.8339	54.78323
19.13527	4.5448	272.1318	58.59104	79.36643	54.78323
40.06849	4.29913	268.6643	59.45086	76.92636	54.90607
60.23116	4.29913	260.9589	60.55635	72.81678	52.44942
68.96404	3.8078	255.565	60.18786	67.93664	52.20375
78.72431	1.47399	248.8869	60.06502	60.10273	51.95809
83.73287	2.70231	243.4931	62.6445	53.6815	51.71242
87.07191	3.31647	239.5119	64.60982	47.77397	51.46676
95.67636	4.5448	233.8612	68.29479	40.58219	50.60693
98.88698	4.66763	226.7979	72.71676	34.03253	49.7471
119.6917	5.52746	219.7345	76.89306	29.02397	48.51878
139.2123	5.40462	214.8544	78.98121	24.78595	47.90462
158.7328	5.03613	211.5154	81.56069	20.67636	46.43063
178.5102	6.38728	206.6352	82.29768	15.02568	44.83381
199.5719	6.38728	193.5359	83.03468	11.30137	43.48265
218.964	6.38728	186.4726	83.40317	7.96233	41.763
239.3835	6.87861	179.0239	83.28034	5.52226	40.41184
259.4178	7.36994	171.3184	83.52601	3.46747	38.32369
267.5085	7.49277	165.7962	83.77167	2.31164	36.11271
275.3424	9.21243	159.375	83.52601	2.18322	34.27023
279.5804	11.30057	154.6232	83.28034	2.18322	32.79624
284.7174	14.12572	149.2294	83.28034	2.82534	31.69075
288.1849	15.35404	142.6797	82.66618	3.46747	29.72543
290.2397	18.17919	140.2397	82.66618	4.10959	28.49711
291.9092	20.26734	136.9006	82.78901	4.62329	27.02312
294.6061	22.23266	132.1489	81.92919	5.00856	25.4263
296.4041	24.6893	128.9383	81.80635	5.13699	24.56647
297.4314	27.14595	125.8561	81.19219	4.62329	24.19797
297.8168	30.09393	123.6729	80.57803	3.59589	23.58381
297.8168	31.81358	122.2602	79.84104	2.69692	22.96965
297.6883	32.67341	120.077	78.48988	1.66952	22.60115
293.5787	32.91907	117.6369	77.13872	0.6421232	22.35549
292.4229	38.56936	116.3527	76.77023	0	20.39017
292.5513	45.9393	114.8116	76.40173	0	14.12572

81 mm in height, and approximately 2 m in the spanwise direction. The spanwise width of the model covers the whole width of the wind tunnel. Due to the fact that the wind tunnel had open side walls, entrainment of the turbulence to the flow was prevented by side walls with height of 30 cm and a length of 2.60 m.

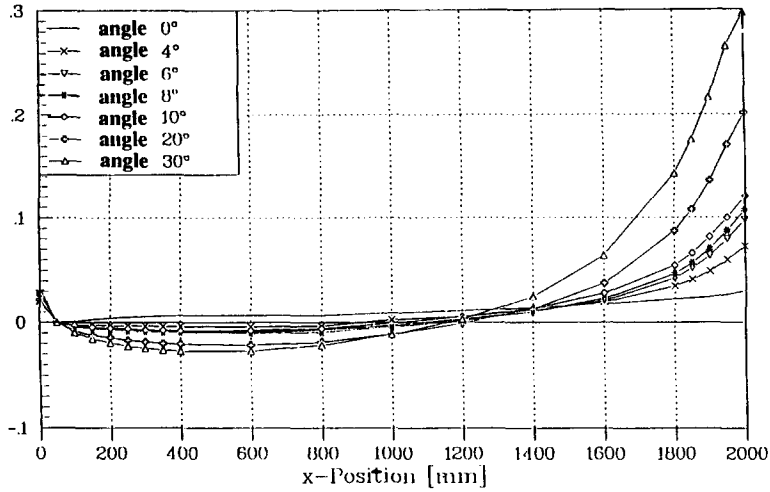

Fig. 4. Static pressure distribution in the middle plane of the wind tunnel for different flap angles.

The model was held by a U-shaped support on both sides and it was free in the air flow without touching the ground and the side walls. As ground under the body, an aluminium plate was installed. The dimensions of the plate were 2.3 m × 2.0 m, and the distance of the plate above the wind tunnel wall was 25 cm. Using the above plate the following characteristics can be achieved:

- The boundary layer at the exit of the wind tunnel nozzle is cut off and disappears under the plate. A thin boundary layer starts to develop at the leading edge of the plate, which has a nose of a NACA 0012 airfoil.
- The plate has a flap at its trailing edge. The angle of attack of this flap can be varied from 0° (horizontal position) to 40°. Using this flap the position of the stagnation point at the leading edge can be changed. An investigation of the static pressure distribution along the plate was initially performed for different flap angles. The preliminary measurements showed (see Fig. 4) that the best results for a symmetric position of the stagnation point at the leading edge, and for the static pressure distribution along the plate (without the model), were achieved for a flap angle of 8°.
- Independently from the characteristics of the boundary layer in the wind tunnel nozzle, the transition point from laminar to turbulent flow can be fixed by a wire.

2.5. *Inlet conditions*

In order to provide the inlet boundary conditions for the numerical simulation, the u, and v velocity components, the turbulence kinetic energy k, and the dissipation rate ε were measured. The measuring positions were located in the spanwise middle plane of the wind tunnel, 30 cm in front of the model, where the inflow boundary of the computational grid was also located.

The dissipation rate was estimated as follows:

The time-average dissipation rate of the turbulence kinetic energy is written as

$$\varepsilon = \nu\overline{\left(\frac{\partial u_i'}{\partial x_k} + \frac{\partial u_k'}{\partial x_i}\right)\frac{\partial u_i'}{\partial x_k}} = \nu\overline{\frac{\partial u_i'}{\partial x_k}\frac{\partial u_i'}{\partial x_k}} + \nu\frac{\partial^2\overline{u_i'u_k'}}{\partial x_i x_k}, \tag{1}$$

and for a free flow, the above equation can be simplified

$$\varepsilon = \nu\overline{\frac{\partial u_i'}{\partial x_k}\frac{\partial u_i'}{\partial x_k}}. \tag{2}$$

With the assumption of local isotropic turbulence, an equation for the isotropic dissipation ε_{is} can be derived:

$$\varepsilon_{is} = 15\nu\overline{\left(\frac{\partial u_i'}{\partial x_k}\right)^2}. \tag{3}$$

Using the Taylor transformation:

$$\bar{u}\frac{\partial(\cdot)}{\partial x} = \frac{\partial(\cdot)}{\partial t}, \tag{4}$$

where $\bar{u}$ is the local mean velocity, and the assumption that the turbulence level of the flow is smaller than 10%, the spatial differentiation can be converted into a time differentiation:

$$\varepsilon = 15\nu\overline{\left(\frac{1}{\bar{u}}\frac{\partial u_i'}{\partial t}\right)^2}. \tag{5}$$

For the determination of the dissipation rate, the flow in the middle plane of the wind tunnel was measured by a boundary layer probe (type DANTEC 55P15). By choosing a sampling frequency of 40 kHz, Kolmogorov's time scale could also be resolved. By taking 100 000 samples per measuring location an accurate estimate of the dissipation rate was obtained

The turbulence kinetic energy was determined from the velocity fluctuations u', v', and w'. An X-wire probe was used, which could be turned around its axial direction. First, the velocity fluctuations in the x–y plane and, subsequently the fluctuations in the x–z plane were measured by turning the proble 90° in the axial direction. The angle calibration was calculated in advance by the preliminary angle calibration of the X-wire probe and under the assumption that the *cosine*-law was valid for the angle dependence of the hot-wire signal.

3. Numerical method

The flow over the car model is described by the incompressible Navier–Stokes equations:

$$\nabla \cdot \boldsymbol{V} = 0, \tag{6}$$

$$\rho \boldsymbol{V} \cdot \nabla \boldsymbol{V} = -\nabla p + \frac{\partial}{\partial x_i}\left[(\mu + \mu_t)\left(\frac{\partial u_i}{\partial x_j} + \frac{\partial u_j}{\partial x_i}\right) - \delta_{ij}\frac{\partial u_k}{\partial x_k}\right], \tag{7}$$

where $\boldsymbol{V}$, p and ρ are the velocity vector, static pressure and density, respectively. The eddy-viscosity, μ_t, is calculated from the turbulence kinetic energy, k, and the dissipation rate, ε, as:

$$\mu_t = \rho C_\mu \frac{k^2}{\varepsilon}, \tag{8}$$

where C_μ is a constant. The values of k and ε are computed using the standard k–ε turbulence model with wall functions [15]. The Navier–Stokes equations are solved by a finite volume pressure correction method of the SIMPLE type. The finite volume discretisation is based on a collocated-grid definition of the variables. The inviscid terms are discretized by a flux-blending scheme [16]. This scheme is based on a combination of first-order upwind discretization and central differences. Second-order central differences are used for the discretisation of the viscous terms. For the solution of the equations an iterative procedure between the velocity and pressure field is obtained. Using an initial approximation for the pressure, the momentum equations are solved to determine the velocity field. The pressure is subsequently corrected by a Poisson equation which is formed by the continuity and momentum equations. Discretisation of this equation results in an algebraic equation of the form:

$$A_p \phi_p + \sum A_{nb} \phi_{nb} = Q, \tag{9}$$

where the index nb runs along the centers of the nearest neighbouring control volumes, and A_{nb} and Q are the coefficients and the source term for each control volume, respectively. For the entire solution domain a matrix equation is formed:

$$\mathbf{A}\,\phi = \mathbf{Q}, \tag{10}$$

where ϕ is the column matrix containing values of the variables on the cell-centroids, $\mathbf{Q}$ is the corresponding column-matrix containing the source term, and $\mathbf{A}$ is the coefficient matrix. The system of equations (10) is written in the following form:

$$\mathbf{M}\,\phi^m = \mathbf{Q} - [\mathbf{A} - \mathbf{M}]\,\phi^{m-1}, \tag{11}$$

where the matrix $\mathbf{M}$ is inverted by a Strong Implicit Procedure (SIP) [17]. The number of inner-iterations for inverting the matrix $\mathbf{M}$ is usually prescribed, otherwise a convergence criterion is defined for terminating the iterative procedure.

In the numerical solution, high frequency errors are damped out within a limited number of iterations. However, the low frequency errors need a large number of

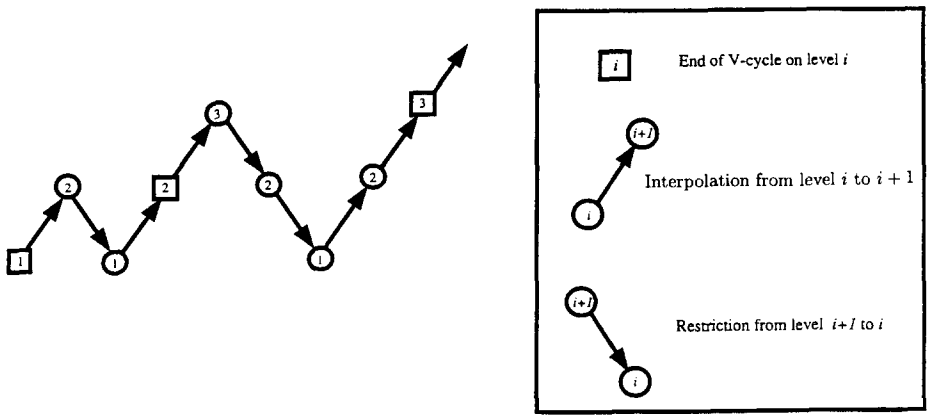

Fig. 5. Schematic representation of a V-multigrid cycle.

iterations for reaching the convergence limit. The estimated computational effort is proportional to N^2, where N is the number of grid points. On the other hand, using multigrid methods the computational effort is almost proportional to N independently of the number of grid points. In the present paper a multigrid method based on the full approximation scheme (FAS) is used [18]. A V-multigrid cycle solution is schematically shown in Fig. 5. The equations are initially solved on a coarse grid, and consequently the solution is interpolated to the next finer grid. The values of the coarse grid are transferred to the fine one through bilinear interpolation. The fine grid intermediate solution is also "restricted" to the coarser level and the coarse-fine grid procedure is repeated until a steady state solution is achieved. For solving the equations in complex geometries the multiblock technique is employed. The computational domain is subdivided into several blocks and the equations are solved on each block, sequentially.

4. Experimental and numerical results

Pressures on the upper and lower surface of the car as well as the u- and v-velocity components at different positions around the car were calculated. The geometry is positioned between $X/L = 0$, and $X/L = 1$, where L is the length of the car. The free stream velocity was taken as 15 m/s and the length of the model as 0.295 m.

Block-structured grids were used and the partitioning of the computational domain into several blocks is shown in Fig. 6. The finer grid was generated from the coarse one through an automatic refinement. Two different grids with 10 000, and 40 000 control volumes were used. An enlargement of these grids around the car is shown in Fig. 7. The minimum grid-spacing in the y-direction was $0.0003L$, and $7.5 \times 10^{-5}L$ for the

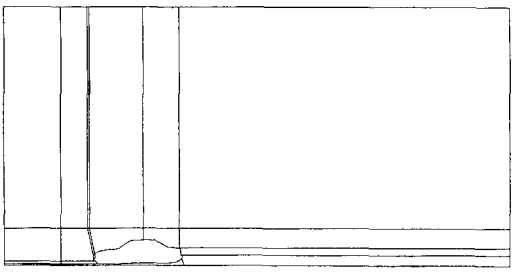

Fig. 6. Multiblock decomposition of the computational domain over the car model.

coarse and the fine grids, respectively. The inflow and outflow boundaries were located one body-length upstream and $4.66L$ downstream. The upper boundary was located $2.6L$ above the body, and the ground-clearance was $0.1L$.

The effect of the grid refinement on the pressure coefficient distribution is shown in Fig. 8. The numerical predictions are compared with the experimental results for the upper and lower surfaces, respectively. In the vertical-front part of the car, a sudden deceleration of the flow takes place, resulting in a rise of the static pressure. The flow then accelerates rapidly as it goes past the leading edge of the bonnet, creating a pressure suction peak. The pressure rises along the bonnet and reaches a local maximum value at the bonnet–windscreen junction. A rapid reduction of pressure follows, and a maximum suction peak occurs at the roof–windscreen junction. The velocity along the roof gradually reduces, resulting in a static pressure rise. At the end of the roof, separation of the flow occurs. The velocity vectors in this region are shown in Fig. 9. Due to the flow separation, pressure recovery does not occur, and a plateau region of pressure appears, as it is indicated from the experiment. In the front half of the lower surface, the velocity gradually increases resulting in a pressure reduction, while in the middle and rear part of the car, a plateau region of pressure exists. The maximum velocity at the lower surface appears at $X/L = 0.3$, resulting in a sharp suction peak similar to that on the upper surface. The numerical predictions are in satisfactory agreement with the experimental results for the front part of the car, but discrepancies are present at the rear of the vehicle where separation of the flow occurs. The pressure distribution is not significantly changed by grid refinement. The main differences between coarse and fine grid results are in the value of the minimum pressure.

In the past, discrepancies between numerical and experimental results for the pressure distribution over car geometries have also been reported by other authors. Show [12] and Hawkins et al. [19] carried out computations over a full scale car-model designed by the Motor Industries Research Association (MIRA), and they compared the numerical predictions with corresponding experimental results. Their computations revealed that the most significant discrepancies were present over the rear screen and boot, where extensive separation of the flow occurred. In addition,

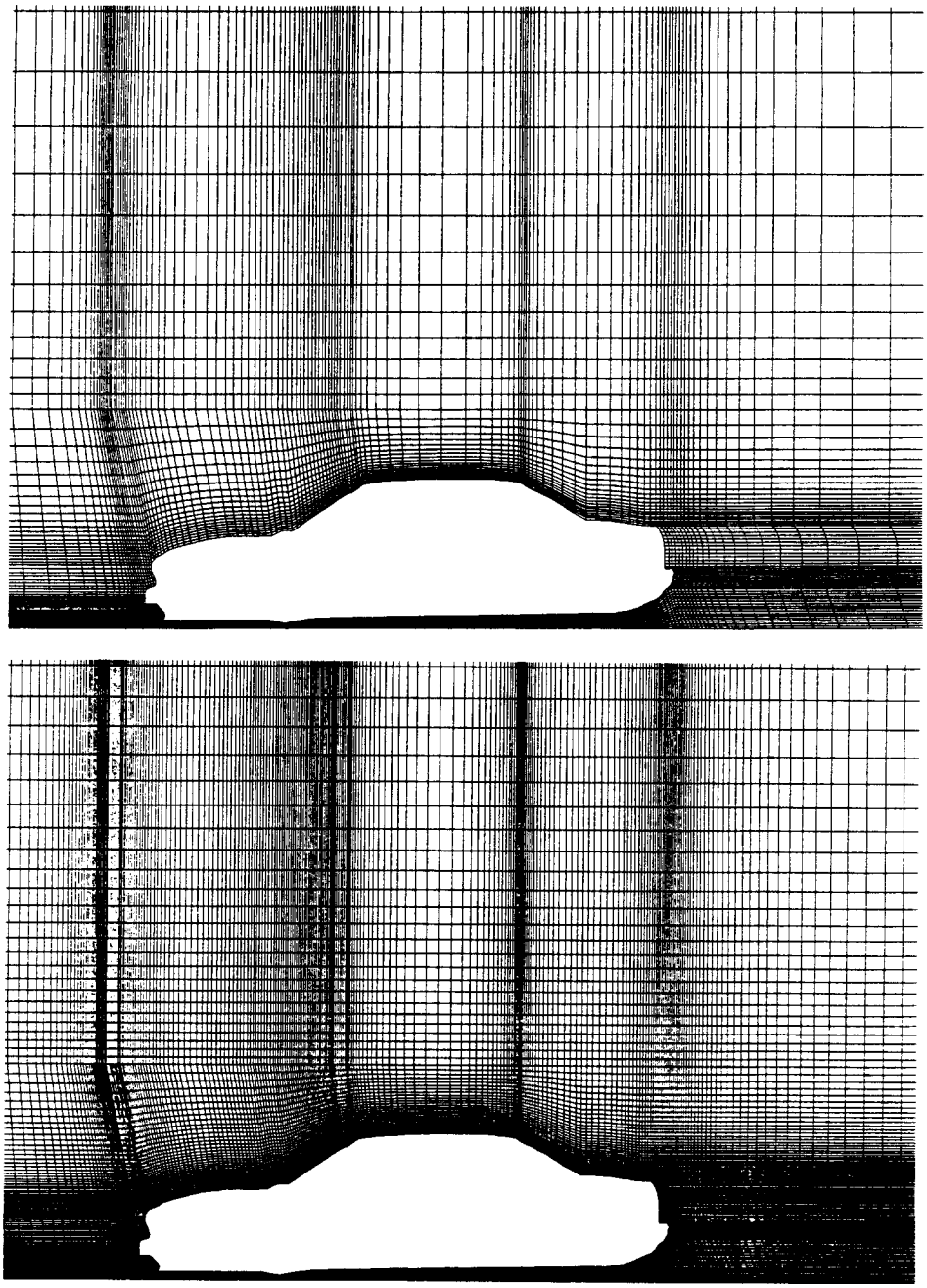

Fig. 7. Enlargement of the coarse and fine grid around the car model.

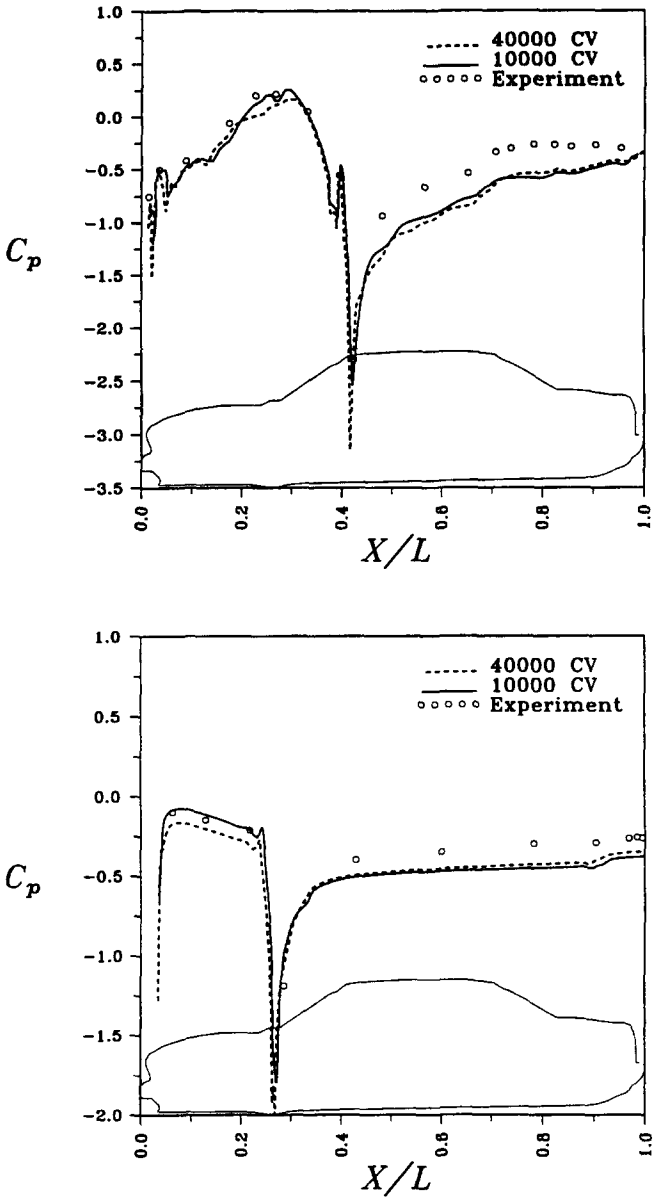

Fig. 8. Comparison of numerical predictions with experimental measurements for the pressure coefficient distribution on the upper (top figure) and lower surface (bottom figure).

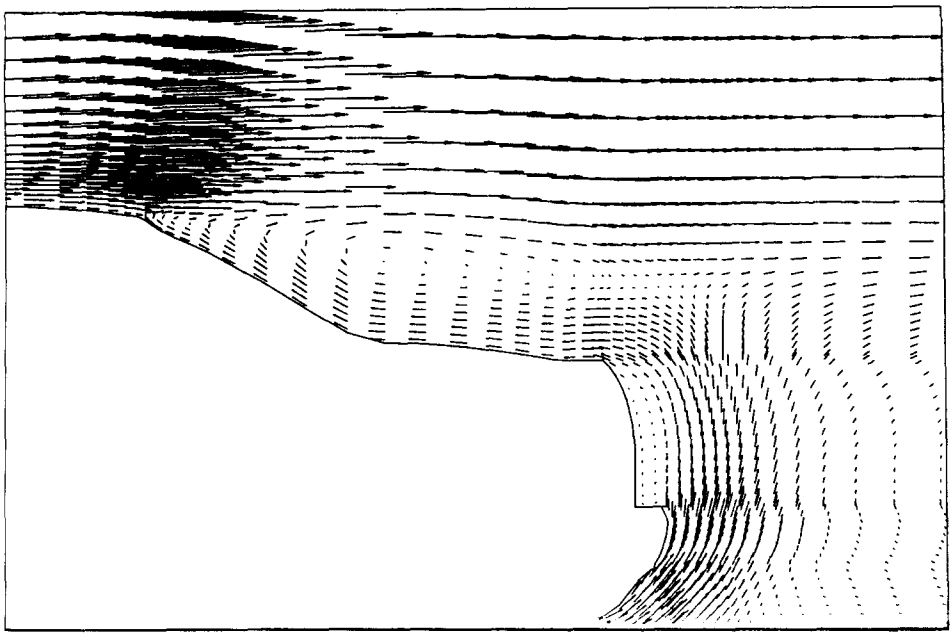

Fig. 9. Velocity vectors in the rear part of the car.

their computations revealed a suction peak that did not appear in the experimental results. They also found that the overall pressure level predicted on the underfloor of the vehicle was not in good agreement with the experiment. Similar discrepancies were also documented in the review articles by Kobayashi et al. [10] and by Himeno et al. [20]. Several reasons were reported as a possible source of errors in the aforementioned studies. The first reason was the coarseness of the grid in both the front and the rear part of the car models. Secondly, it was reported that the discretisation scheme for the convection terms may cause high numerical diffusion, and this is an area for further investigation. Finally, the inaccuracies introduced by the turbulence modelling are certainly one of the most important sources of error. In the present study, a standard k–ε model with wall functions was used. The implementation of low-Re two-equation models and second-moment closures is another area for further investigation.

In Figs. 10 and 11 comparisons of the numerical predictions with the experimental results for the u-, and v-velocity components are shown, respectively. In general, the numerical predictions are in qualitative agreement with the experiment. The results for the coarse and fine grids do not show significant differences, except in some cases for the v-velocity profile. Satisfactory agreement between numerical predictions and experimental measurements are obtained in the near wall region,

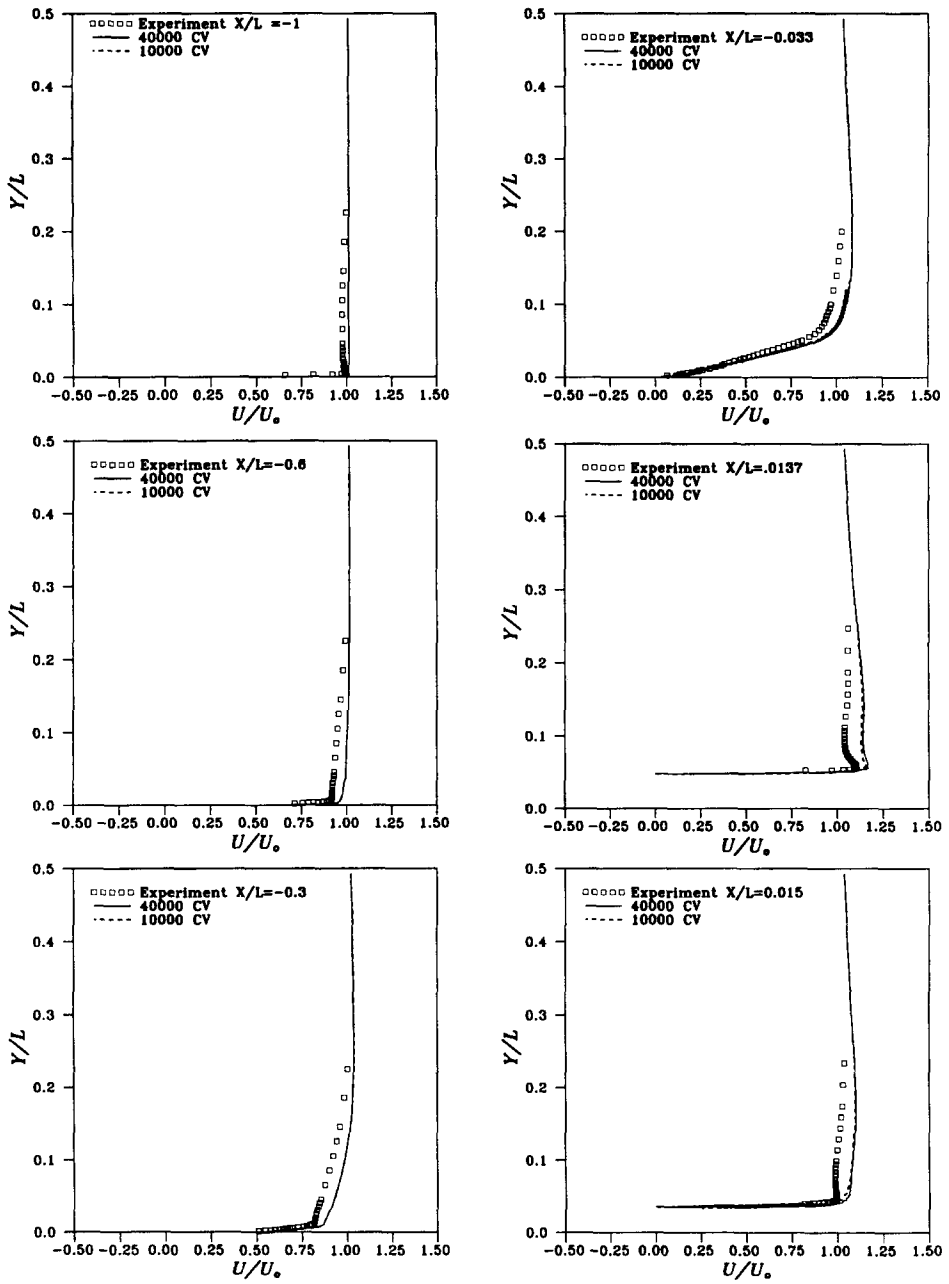

Fig. 10. Comparison of numerical predictions with experimental measurements for the u velocity at various X/L positions around the car.

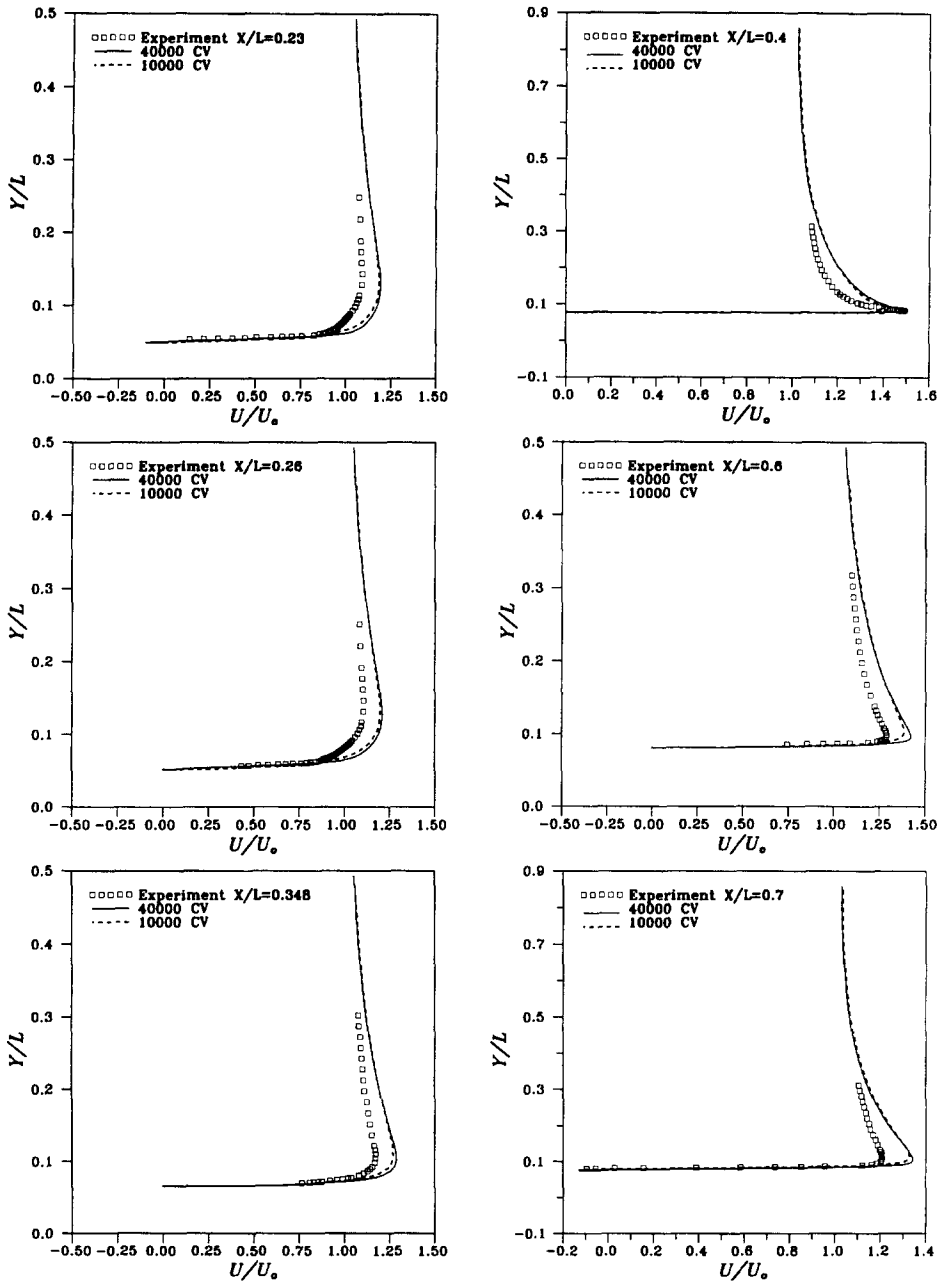

Fig. 10. Continued.

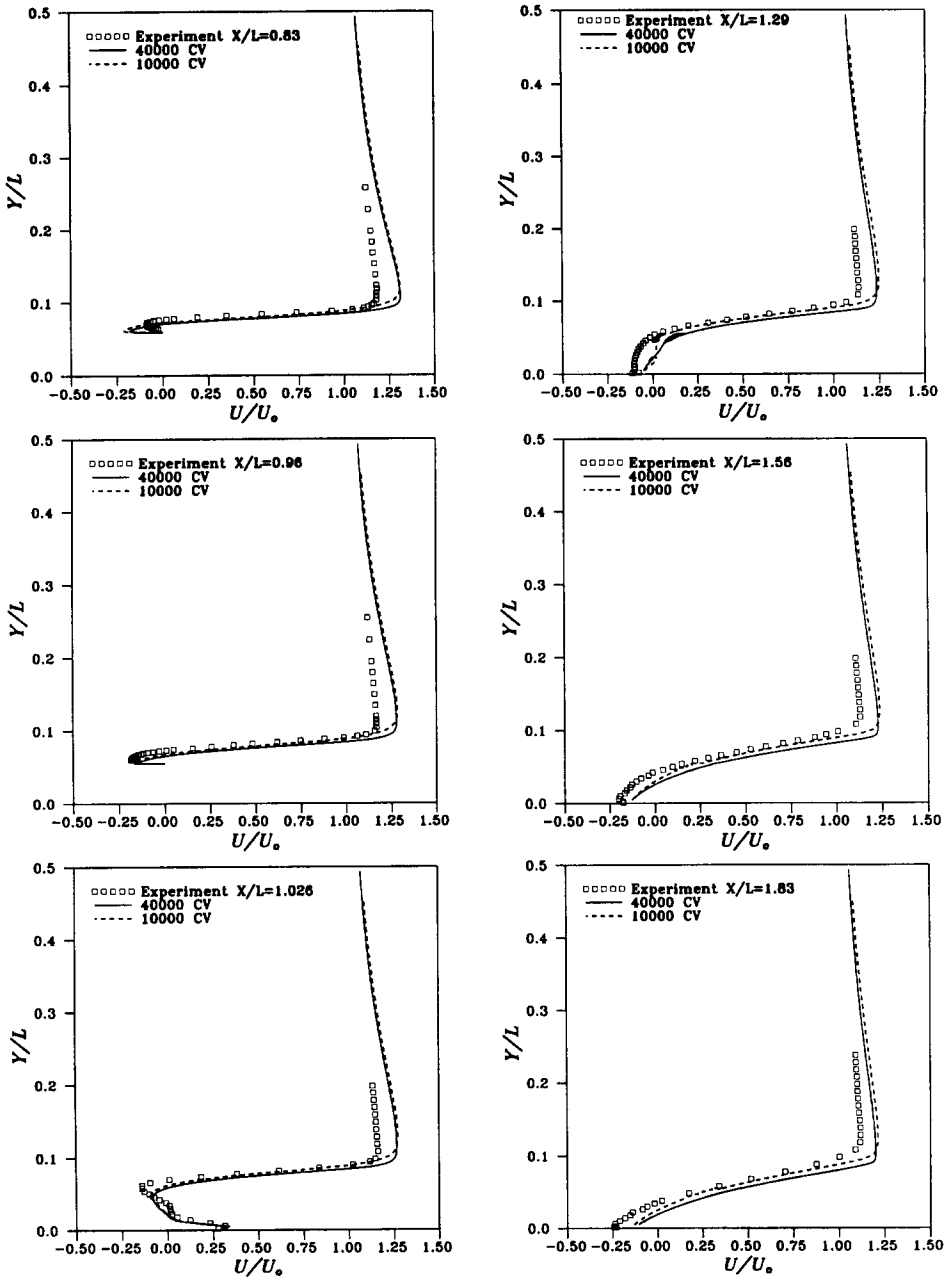

Fig. 10. Continued.

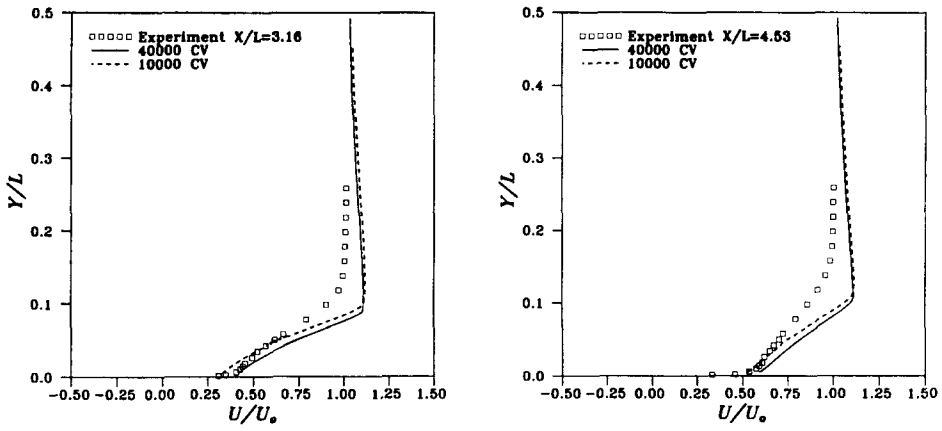

Fig. 10. Continued.

Table 3
Computing time using the multigrid and the single grid solutions for computations on 10000 (grid 1) and 40000 control volumes (grid 2)

	Grid 1 (h)	Grid 2 (h)
Single grid	3	30
Multigrid	0.6	6.5

but the computations overestimate the velocity profile in the outer region of the boundary layer, especially in the middle and rear part of the car. The discrepancies between numerical and experimental results may be due to the turbulence model and numerical scheme used. The objective of the present paper is neither to assess different discretization schemes nor to improve the turbulence model, but to show the limits of the present numerical algorithm and turbulence model.

The multigrid method provides an acceleration factor of 4–5. The computing time for the coarse and fine grids is shown in Table 3. The computations were performed on a SUN 10/20 workstation.

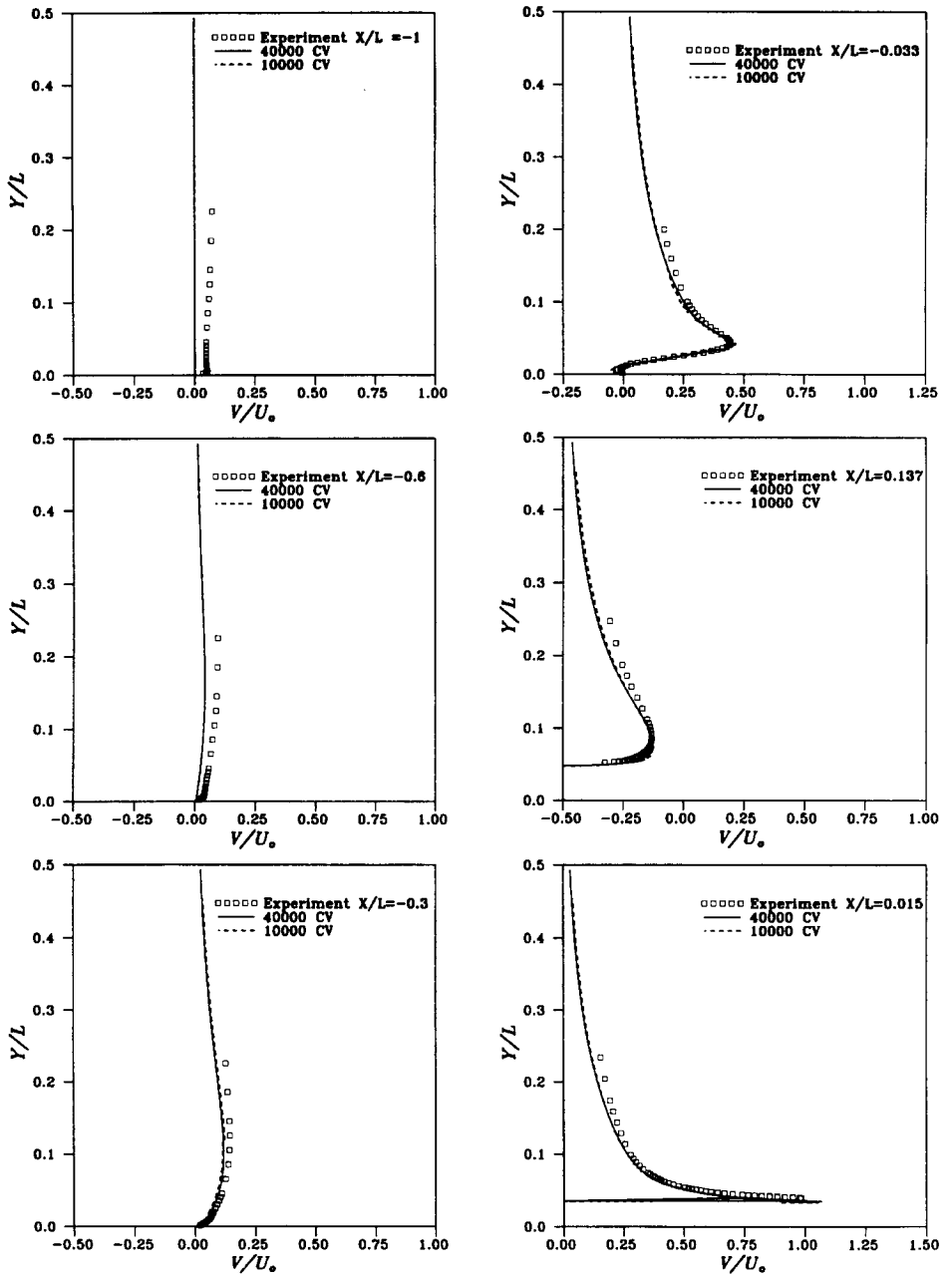

Fig. 11. Comparison of numerical predictions with experimental measurements for the v velocity at various X/L positions around the car.

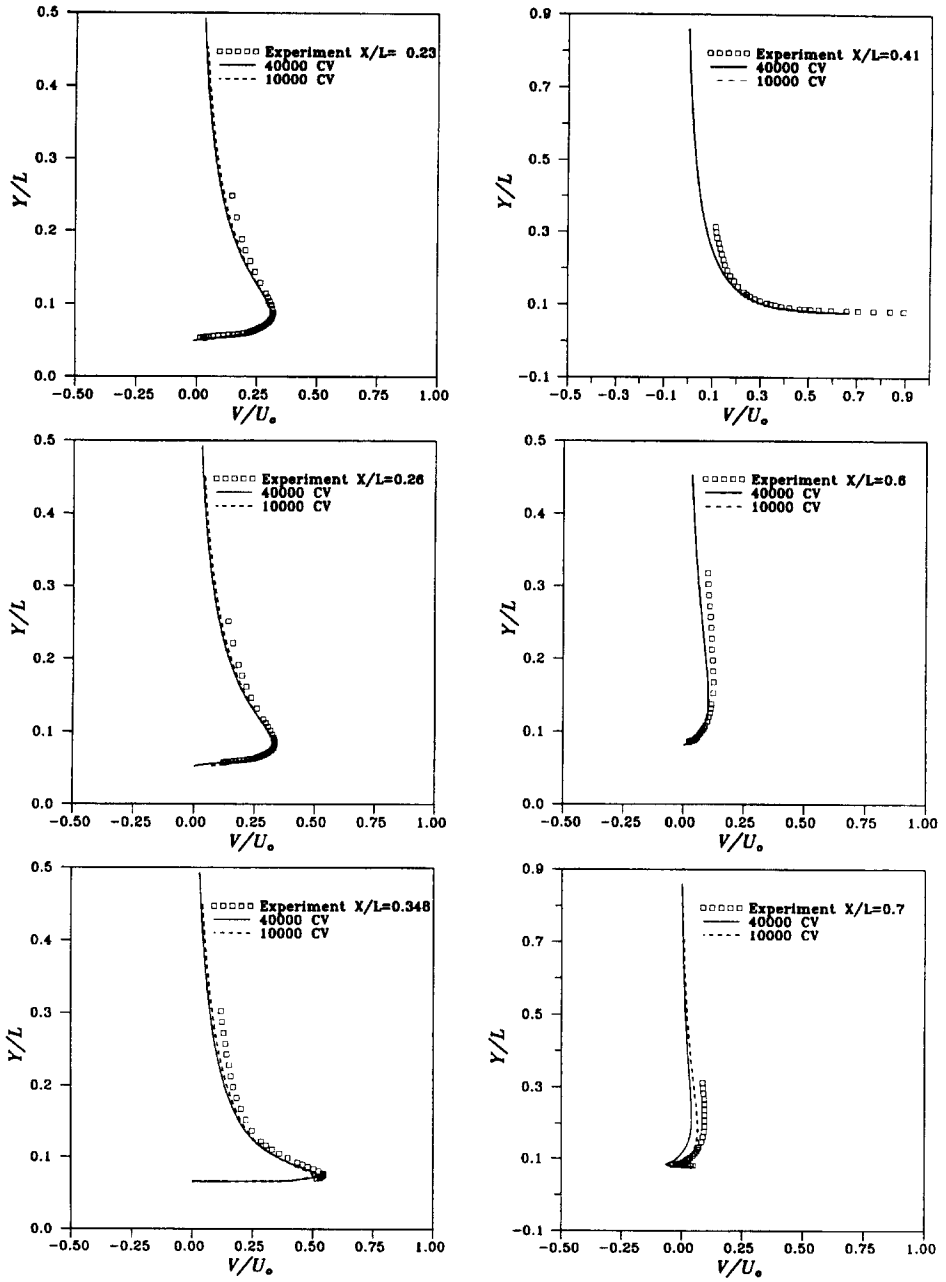

Fig. 11. Continued.

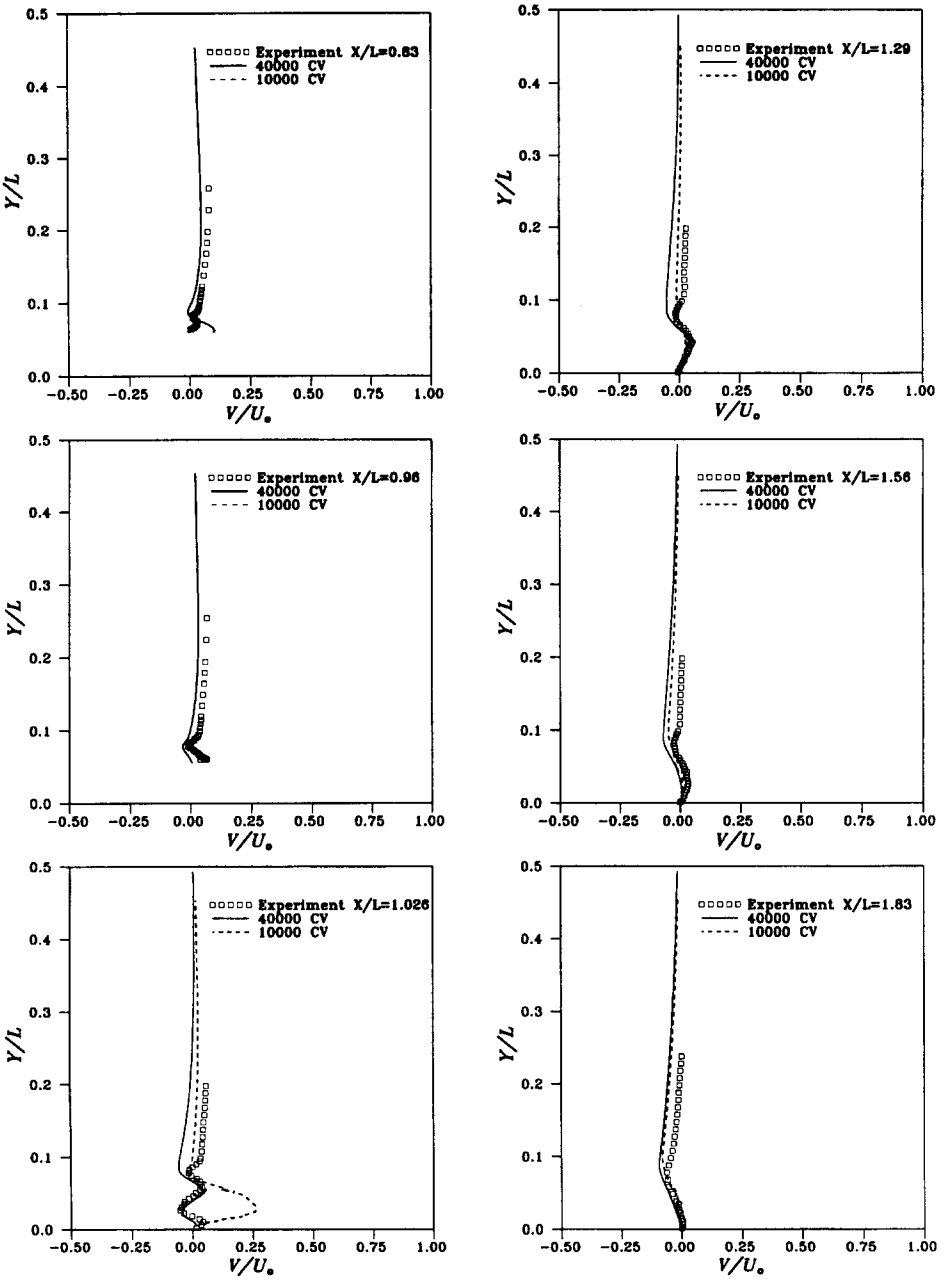

Fig. 11. Continued.

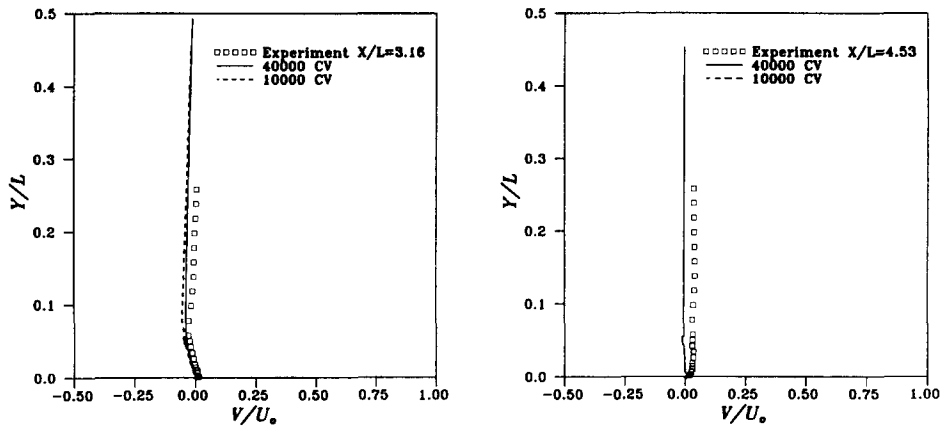

Fig. 11. Continued.

5. Conclusions

A joint experimental-numerical study of the flow over a two-dimensional car model was presented. The computations were carried out using a pressure correction algorithm in conjunction with a multigrid method and the k–ε turbulence model. Experiments for the pressure distribution and the velocity profiles were also performed. The basic conclusions from the above study are summarised, as follows:

- The computations are in qualitative agreement with the experimental measurements for both the pressure and velocity profiles.
- Discrepancies between predicted and measured values of the pressure appear in the middle and rear part of the model.
- The numerical method predicts satisfactorily the velocity distribution in the near wall region, but overestimates the velocity values in the outer region of the boundary layer.
- The multigrid method can be efficiently used for such computations providing an acceleration factor of 4 to 5.
- The grid refinement does not significantly change the structure of the computed flow field. The discrepancies between predictions and experiment may be mainly due to the turbulence model and numerical method used.
- Advanced turbulence models and high-order numerical discretisation have to be investigated in the future for flows over car geometries. Experimental measurements over three-dimensional models need also to be performed.

Acknowledgements

The numerical study was financially supported by CEC through the COPERNICUS project (COP-1294). The authors would like to thank Mr. G. Rokonal for his valuable help during the preparation and execution of experiments. Authors are listed alphabetically.

References

[1] P.W. Bearman, J.P. Davis and J.K. Harvey, Wind tunnel investigation of vehicle wakes, in: Proc. Vehicle Aerodynamics Symp., sponsored by Volkswagenwerk AG-Research Division (1982).
[2] W.H. Hucho, Aerodynamics of Road Vehicles (Butterworth-Heinemann, London, 1987).
[3] P.W. Bearman, Some observations on road vehicle wakes, SAE paper 840301, SAE Internat. Congr. and Exposition (1984).
[4] M. Rauser and J. Eberius, Verbesserung der Fahrzeugaerodynamik durch Unterbodengestaltung, Automobiltechnische Zeitschrift 89(10) (1987) 535–539.
[5] S.R. Ahmed, Wake structure of typical automobile shapes, Trans. ASME, J. Fluids Eng. 103 (1981) 162–169.
[6] S.R. Ahmed, Influence of base slant on the wake structure and drag of road vehicles, Trans. ASME, J. Fluids Eng. 105 (1983) 429–434.
[7] S.R Ahmed, G. Ramm and G. Faltin, Some salient features of the time-average ground vehicle wake, SAE paper 840300, SAE Internat. Congr. and Exposition (1984).
[8] F. Durst, A. Melling and J.H. Whitelaw, Principles and practice of laser-doppler anemometry (Academic Press, London, 1976).
[9] M. Takagi, Application of computers to automobile aerodynamics, J. Wind Eng. Ind. Aerodyn. 33 (1990) 419–428.
[10]. T. Kobayashi and K. Kitoh, A review of CFD methods and their application to automobile aerodynamics, SAE paper 920338, SAE Internat. Congr. and Exposition (1992).
[11] H. Rieger, F. Magagnato, W. Fritz and W. Seibert, Numerical simulation of turbulent flows around complex car shapes – experiences, status and outlook, VDI Berichte 1007 (1992).
[12] C.T. Shaw, Predicting vehicle aerodynamics using computational fluid dynamics – a user's perspective, SAE paper 880455, SAE Internat. Congr. and Exposition (1988).
[13] T. Han, Computational analysis of three-dimensional turbulent flow around a bluff body in ground proximity, AIAA J. 27(9) (1989) 1213–1219.
[14] W. Angelis and G. Rokonal, Komplementäre Methodik in der Aerodynamik Bodennaher Fahrzeuge, DGLR Konferenz, Erlangen (1994).
[15] B.E. Launder and D.B. Spalding, Mathematical Models of Turbulence (Academic, New York, 1972).
[16] I. Demirdzic and M. Peric, Finite volume methods for prediction of fluid flow in arbitrary shaped domains with moving boundaries, Int. J. Numer. Methods Fluids 10 (1990) 771–790.
[17] H.L. Stone, Iterative solution of implicit approximations of multi-dimensional partial differential equations, SIAM J. Numer. Anal. 5 (1968) 530–558.
[18] M. Hortmann, M. Peric and G. Scheuerer, Finite volume multigrid prediction of laminar convection: Benchmark solutions, Int. J. Numer. Methods Fluids 11 (1990) 189–207.
[19] I.R. Hawkins, A. Honecker, H. Krus, C.T. Shaw and S. Simcox, Numerical studies of vehicle aerodynamics, SAE paper 905129, SAE Internat. Congr. and Exposition (1990).
[20] R. Himeno, M. Takagi, K. Fujitani and H. Tanaka, Numerical analysis of the airflow around automobiles using multi-block structured grids, SAE paper 900319, SAE Internat. Congr. and Exposition (1990).